DEEP INELASTIC LEPTON SCATTERING IN NUCLEI AT $x > 1$ AND THE NUCLEON SPECTRAL FUNCTION

P. Fernández de Córdoba, E. Marco, H. Müther, E. Oset and Amand Faessler

Institut für Theoretische Physik, Universität Tübingen, 72076 Tübingen, Germany.

Abstract

The nuclear structure function $F_{2A}(x)$ has been studied in the Bjorken limit for (l, l') scattering on nuclei in the region of $x > 1$ and was found to be very sensitive to the information contained in the nucleon spectral function in nuclei, particularly the correlations between momenta and energies in the region of large momenta. Calculations were done in a local density approximation using two different spectral functions for nuclear matter. Results are compared to those obtained for a spectral function which has been evaluated directly for the finite nucleus, ^{16}O, under consideration. For values of x around 1.5 and larger the quasiparticle contribution is negligible, thus stressing the sensitivity of the present reaction to the dynamical properties of nuclei beyond the shell model approach. Several approximations which are usually employed in studies of the EMC effect have been analyzed and their inaccuracy in this region is demonstrated. The results stress the fact that the nuclear structure function contains important information on nuclear dynamical correlations. Therefore further measurements of $F_{2A}(x)$ in that region and for many nuclei would be most welcome.

1 Introduction

Deep inelastic scattering of leptons on nuclei in the region of asymptotic freedom and the ratio $R(x)$ of the nuclear structure function compared to the corresponding one for the deuteron (EMC effect [1]) has been one of the topics in the interface of nuclear and particle physics intensively studied in the recent past [2–5]. After multiple discussions, pionic effects [4, 6–8], binding effects [9–11] and Fermi motion [3, 6, 12] have turned out to be important ingredients to describe the main characteristics of the ratio $R(x)$: the small enhancement beyond unity around $x \simeq 0.1$, the small depletion around $x \simeq 0.6$ and the steady increase around $x \simeq 0.8$ and above, respectively.

The increase of $R(x)$ at x close to one was soon identified to be a consequence of Fermi motion [3, 6, 12] and this is one of the points where there seems to be consensus among scientists. Probably the lack of controversy on this issue prevented a systematic exploration of the region of $x > 1$, in spite of the fact that in nuclei only the variable $x_A = -q^2/2M_A q^0$ is limited between 0 and 1, while $x = -q^2/2Mq^0$ varies from 0 to M_A/M. Since $F_{2N}(x)$, the structure function of a free nucleon, is zero for $x > 1$, the fact that $F_{2A}(x)$ is different from zero for $x > 1$ must necessarily be attributed to modifications of the nucleon properties inside nuclei, i.e. to genuine many body effects. The region of $x > 1$ is hence a source of very interesting information on nuclear properties, as we shall see.

The fact that Fermi motion was so important at $x \simeq 1$ induced people to investigate the region of $x > 1$ with the same idea [11–14]. These works essentially employed phenomenological nuclear matter momentum distributions, with the main conclusion that a nonvanishing value of $F_{2A}(x)$ for $x > 1+k_F/M$ (with k_F the Fermi momentum) would require a tail in the momentum distribution $n(\vec{k})$ for $k > k_F$. The occupation number $n(\vec{k})$ is different from zero for $k > k_F$ as soon as the effects of a residual NN interaction are considered leading to a correlated many-body system of Fermions.

However, it is quite dangerous to reduce the effects of correlations to a discussion of a momentum distribution only, because in a system of interacting Fermions the energy and momentum distributions are correlated by means of the spectral function, and the simultaneous consideration of both distributions is necessary in principle, and also in the practice of the present case, as we shall see. Disregarding the energy and momentum correlations leads sometimes to quite erroneous results, like in the study of the Λ mesonic decay in nuclei where the results for the width based exclusively on the nucleon momentum distribution in nuclei are three orders of magnitude bigger than the results obtained with a spectral function, or the experimental results [15]. The same warning, in the present context, was raised in ref. [16] where $F_{2A}(x)$ was evaluated for ^3He. Further work in this direction was done in refs. [17–19].

In the present work we have evaluated $F_{2A}(x)$ for several nuclei by using spectral functions of infinite nuclear matter and the local density approximation. This approximation is good when dealing with volume processes like the

present one. In order to quantify uncertainties from the many body approach used, we have performed the calculations using two spectral functions evaluated with rather different methods. On the other hand, since large momentum components are necessarily involved in the process, relativistic corrections are bound to be relevant [20,21] and we have worked within a relativistic approach.

We evaluate $F_{2A}(x)$ for values of $1 \leq x \leq 1.5$. At $x = 1.5$ the value of the structure function decreases by about three orders of magnitude with respect to $x = 1$, but is still well within measurable range. We also show results using the momentum distributions alone, within several approximations, and find appreciable differences (of two or more orders of magnitude) with respect to the accurate results using the spectral functions. These results show that the study of nuclear structure functions at values of $x > 1$ is a very interesting tool to learn about nuclear dynamical correlations beyond the nuclear properties described in a shell model approach.

In this paper we not only discuss results obtained within the local density approximation but also consider a spectral function calculated directly for the nucleus ^{16}O. After this introduction we discuss in section 2 the calculation of the nuclear structure function and its relation to the spectral function. The various approaches for the spectral functions are presented in section 3. The results of our studies are presented and discussed in section 4. The last section summarizes the main conclusions.

2 The nuclear structure function

Deep inelastic electron (or muon) scattering on an unpolarized nucleon can be described in terms of two structure functions, $W_1(x, Q^2)$, $W_2(x, Q^2)$, where the Bjorken variable x is given by

$$x = \frac{-q^2}{2pq} = \frac{Q^2}{2pq} \tag{1}$$

with q the momentum of the virtual photon and p the momentum of the nucleon. In the Bjorken limit, $q^0 \to \infty$, $Q^2 \to \infty$ and x fixed, it is common to define the structure functions F_1 and F_2 which depend only on the variable x, up to some smooth logarithmic dependence on Q^2 from QCD corrections. In this limit one has

$$\begin{aligned} \tfrac{p.q}{M} W_2(x, Q^2) &\equiv F_2(x) \\ M W_1(x, Q^2) &\equiv F_1(x) \end{aligned} \tag{2}$$

and $F_2(x)$, $F_1(x)$ are related by the Callan-Gross relation

$$2xF_1(x) = F_2(x) \tag{3}$$

Using these structure functions W_1 and W_2 the hadronic tensor for the absorption of the virtual photon can be written:

$$W'^{\mu\nu} = (-g^{\mu\nu} + \frac{q^\mu q^\nu}{q^2})W_1 + p'^\mu p'^\nu \frac{W_2}{M^2}$$

$$p'^\mu = p^\mu - \frac{p.q}{q^2} q^\mu \tag{4}$$

It is practical to work in a frame where $\vec{q}$ is parallel to the z direction. Adopting this frame and inspecting the transversal W'^{xx} component in the Bjorken limit, one finds that the term proportional to W_2 in eq. (4) vanishes and W'^{xx} is related to W_1 for nucleons in nuclei with the same coefficient in front as for one nucleon in the vacuum, independent on its momentum or energy. This allows one to write the structure function F_{1A} derived from lepton scattering from a nucleus with baryon number A in a nonrelativistic formalism using eq. (2).

$$\frac{F_{1A}(x_A)}{M_A} = \int \frac{d^3p}{(2\pi)^3} \int_{-\infty}^{\mu} d\omega \, \mathcal{S}_h(\omega, p) \frac{F_{1N}(x_N)}{M} \theta(x_N) \, \theta(1 - x_N) \tag{5}$$

where $\mathcal{S}_h(\omega, p)$ denotes the hole spectral function, i.e. the probability of finding a nucleon with energy ω and momentum p in the nucleus, the integration limit μ the chemical potential or Fermi energy and

$$x_A = \frac{-q^2}{2p_A q} = \frac{-q^2}{2M_A q^0}\,; \quad x_N = \frac{-q^2}{2pq}\,; \quad p \equiv (\omega, \vec{p}) \tag{6}$$

Instead of x_A one normally uses the variable x,

$$x = \frac{-q^2}{2Mq^0} = \frac{M_A}{M} x_A \tag{7}$$

so we will write F_{1A} and F_{2A} as functions of x from now on.

By means of eq. (3) for nuclear targets we can calculate F_{2A} which is the structure function used in studies of the EMC effect. We then write

$$F_{2A}(x) = \int \frac{d^3p}{(2\pi)^3} \int_{-\infty}^{\mu} \mathcal{S}_h(\omega, p) \frac{x}{x_N} F_{2N}(x_N) \theta(x_N) \theta(1 - x_N) \tag{8}$$

Instead of using the spectral function $\mathcal{S}_h$ calculated directly for the nucleus under consideration, it is common practice to employ a local density approximation and represent this spectral function in terms of a spectral function $S_h(\omega, p; \rho)$ evaluated for infinite nuclear matter at various densities ρ which is normalized by

$$4 \int \frac{d^3p}{(2\pi)^3} \int_{-\infty}^{\mu} d\omega \; S_h(\omega, p; \rho) = \rho \,, \tag{9}$$

with a factor 4 on the left side of this equation to account for the spin-isospin degeneracy of symmetric nuclear matter. Assuming a density profile $\rho(r)$ for the finite nucleus to be studied, one can determine the local density approximation for the spectral function of this nucleus by

$$\mathcal{S}_h(\omega,p) = 4\int d^3r S_h\left(\omega,p;\rho(r)\right) \tag{10}$$

which ensures that

$$4\int d^3r \int \frac{d^3p}{(2\pi)^3}\int_{-\infty}^{\mu} d\omega\ S_h\left(\omega,p;\rho(r)\right) = \int \frac{d^3p}{(2\pi)^3}\int_{-\infty}^{\mu} d\omega\ \mathcal{S}_h(\omega,p) = A\ . \tag{11}$$

For nuclear matter the spectral function can be evaluated in terms of the nucleon selfenergy $\Sigma(\omega,p)$ by

$$S_h(\omega,p) = \frac{1}{\pi}\frac{Im\Sigma(\omega,p)}{[\omega-\varepsilon(\vec{p})-Re\Sigma(\omega,p)]^2+[Im\Sigma(\omega,p)]^2} \tag{12}$$

where we have dropped the variable ρ identifying the density dependence of the self-energy and spectral function. In eq. (12), $\varepsilon(\vec{p})$ is used to represent the nucleon kinetic energy.

Relativistic corrections accounting for the kinematics of the nucleon have been included in deep inelastic scattering. Prescriptions based on the normalization of the relativistic current operator lead to corrections of the static, or shell model, structure function of the nucleus [22]. Further corrections have been considered in [20, 21] at $x \simeq 1$. In ref. [23] a different relativistic treatment is developed which allows to write all quantities in terms of the nucleon propagators. Only the region $0 < x < 1$, which was measured by the EMC collaboration, is studied there. As in ref. [4, 6, 7], pionic corrections are shown to be relevant in the region of $x < 0.6$, but they play no role in the region $x > 1$ which we study here.

Employing the treatment described in ref. [23], which uses a relativistic spectral function from the beginning, one can avoid introducing any flux factors as in ref. [22] to account for relativistic corrections in non-relativistic nuclear wave functions.

Since the relativistic corrections are important here we take advantage to discuss briefly and complement the details of ref. [23].

In fig. 1a we show the Feynman diagram that symbolizes the deep inelastic process on a nucleon. The final hadronic state X will contain at least one baryon and will have baryonic number one. In a nucleus the nucleon N will have a certain momentum and energy distribution given by the spectral function. The most practical way to take this into account and have a covariant formulation of the nuclear problem is to fold the amplitude in fig. 1a and convert it into a many body diagram for the selfenergy of an electron in the nuclear medium, fig. 1b. Here the nucleon N in fig. 1a gets converted into a hole line and with the baryon existing in X it completes a fermionic loop. In section 3 of ref. [23] one evaluates this selfenergy in infinite nuclear matter and, by means of the local density approximation, the (e,e') cross section, is related to the imaginary part of the electron selfenergy. The imaginary part of the e

selfenergy is evaluated using Cutkosky rules and this means that the intermediate states e' and X are placed on shell in the integrations over the momenta of these states. The formalism is originally covariant in the sense that everything is written in terms of propagators of the particles and we can write the nucleon propagator in a covariant relativistic way. However, Cutkosky rules select the imaginary part of the propagator of nucleon N for the occupied states and when doing that the apparent covariant structure might not show up clearly.

In our formalism we start from a free nucleon propagator which we split into its positive and negative energy parts [24]

$$\frac{\not{p}+M}{p^2-M^2+i\epsilon} \equiv \frac{M}{E(\vec{p})}\left\{\frac{\sum_r u_r(\vec{p})\bar{u}_r(\vec{p})}{p^0-E(\vec{p})+i\epsilon}+\frac{\sum_r v_r(-\vec{p})\bar{v}_r(-\vec{p})}{p^0+E(\vec{p})-i\epsilon}\right\} \tag{13}$$

where $M, E(\vec{p})$ are the nucleon mass and the relativistic nucleon energy $(\vec{p}^{\,2}+M^2)^{1/2}$ and $u_r(\vec{p})\,,\, v_r(\vec{p})$ are the ordinary spinors which we take normalized as $\bar{u}_r(\vec{p})u_r(\vec{p})=1$. We recall that $u_r(\vec{r})$ are functions of three momentum and they are the only spinors which appear in our framework.

In order to account for binding and momentum distribution of the occupied nucleons we need the nucleon propagator in the nucleon medium.

Note that even if a nucleon is off shell, $p^0 \neq E(\vec{p})$, in the propagator of eq. (13) and we have $\not{p}+M \to p^0\gamma^0-\vec{p}\vec{\gamma}+M$, the positive energy part has the Dirac structure $2M\sum_r u_r(\vec{p})\vec{u}_r(\vec{p}) = E(\vec{p})\gamma^0-\vec{p}\vec{\gamma}+M$, corresponding to on shell nucleons of momentum $\vec{p}$.

Following a standard relativistic notation [25] the nucleon propagator in a spin saturated system would be

$$G(p^0,p)=\frac{1}{\not{p}-M-\Sigma^s-\Sigma^v\gamma^0} \tag{14}$$

which includes a scalar and vector terms in the nucleon selfenergy (the inclusion of a term of the type $\vec{\gamma}\vec{p}$ does not change the arguments and conclusions which follow). The extraction of hole and particle spectral functions requires the evaluation of $Re\Sigma^{s,v}$ and particularly $Im\Sigma^{s,v}$, which is a non trivial task.

We respect the structure of eq. (14) but follow a different path in order to single out the imaginary part of the positive energy piece of the nucleon propagator. We start from the realization that for this latter purpose, in a perturbative expansion of the propagator of eq. (14) in terms of the free propagator of eq. (13), the terms of positive energy will be singular and dominate over those of negative energy. This allows us to write the desired part of the propagator as

$$\tilde{G}(p^0,p)=\frac{M}{E(\vec{p})}\sum_r u_r(\vec{p})\bar{u}_r(\vec{p})\frac{1}{p^0-E(\vec{p})}+$$

$$\frac{M}{E(\vec{p})}\sum_r \frac{u_r(\vec{p})\bar{u}_r(\vec{p})}{p^0-E(\vec{p})}\Sigma(p^0,p)\frac{M}{E(\vec{p})}\sum_s \frac{u_s(\vec{p})\bar{u}_s(\vec{p})}{p^0-E(\vec{p})}+...$$

$$= \frac{M}{E(\vec{p})} \sum_r \frac{u_r(\vec{p})\bar{u}_r(\vec{p})}{p^0 - E(\vec{p}) - \bar{u}_r(\vec{p})\Sigma(p^0,p)u_r(\vec{p})\frac{M}{E(\vec{p})}} \tag{15}$$

This expansion is rather useful because both Σ^s and $\Sigma^v\gamma^0$(and $\vec{\gamma}\vec{p}$) are diagonal in the base of the $u_r(\vec{p})$ spinors, which converts eq. (15) in an ordinary geometric series, not a matricial series, which can be summed trivially as shown in the last step of eq. (15).

It might look surprising that one obtains a Dirac structure $u_r(\vec{p})\bar{u}(\vec{p})$ in $\tilde{G}(p^0,p)$ as for free nucleons, even when the renormalized nucleons will be off shell. This is less striking if one recalls that also in eq. (13) the positive energy part (corresponding to $\tilde{G}$) has the same structure $u_r(\vec{p})\vec{u}_r(\vec{p})$ even if the nucleon is off shell. In any case the structure might not match the one coming from eq. (14) and one has lost the covariance shown by eq. (14). The reason for this loss of covariance is that one loses terms with admixture of the positive and negative parts of the nucleon propagator of eq. (13) in the perturbative exapansion. This is, in the sum of eq. (15) one is summing terms of the type of fig. 2a,b,c,d, where in the intermediate fermion lines one only has the part of positive energy of the propagator. One is missing terms of the type of fig. 2e (where the line pointing down stands for the negative energy part of the free nucleon propagator), which would naturally appear in a covariant expansion of eq. (14).

On the other hand while all the terms of fig. 2c,d etc. are summed up automatically in eq. (15) in terms of a selfenergy given exclusively by the term in fig. 2b, the second order terms of fig. 2e is not accounted for. We argued that this latter term (which has an intermediate propagator of order 1/2M, and is of ρ^2 type) should be small with respect to the diagrams contained in figs. 2b, c, d, ... But in any case it can be included as a nucleon selfenergy part in the sum of eq. (15) and then diagrams e,f, etc. would be automatically included. This means that even if the covariance is lost in eq. (15) one can still regain all the terms in the series by including these mixed terms in the selfenergy Σ appearing in eq. (15). Of course, this selfenergy is now different to the one appearing in eq. (14). These mixed terms are also diagonal in $u_r(\vec{p})$ and do not change the structure of eq. (15). This is the philosophy which we follow, only that the diagrams of fig. 2e, 2f are not evaluated, although they are implicitly accounted for as we pass to discuss. The reason is that these diagrams only contribute to the real part of Σ, not to the imaginary part, and in our scheme, which evaluates accurately $Im\Sigma$, there are pieces missing in the real part of Σ which are added phenomenologically in order to ensure the exact experimental binding energy of each nucleus [23]. The particular structure of eq. (15) allows one to write

$$\tilde{G}(p^0,p) = \frac{M}{E(\vec{p})} \sum_r u_r(\vec{p})\bar{u}_r(\vec{p})[\int_{-\infty}^{\mu} d\omega \frac{S_h(\omega,p)}{p^0 - \omega - i\eta}$$

$$+\int_{\mu}^{\infty} d\omega \frac{S_p(\omega,p)}{p^0-\omega+i\eta}] \tag{16}$$

with the relationships

$$S_h(p^0,p) = \frac{1}{\pi}\frac{\frac{M}{E(\vec{p})}Im\Sigma(p^0,p)}{[p^0-E(\vec{p})-\frac{M}{E(\vec{p})}Re\Sigma(p^0,p)]^2+[\frac{M}{E(\vec{p})}Im\Sigma(p^0,p)]^2} \quad \text{for } p^0 \leq \mu$$

$$S_h(p^0,p) = -\frac{1}{\pi}\frac{\frac{M}{E(\vec{p})}Im\Sigma(p^0,p)}{[p^0-E(\vec{p})-\frac{M}{E(\vec{p})}Re\Sigma(p^0,p)]^2+[\frac{M}{E(\vec{p})}Im\Sigma(p^0,p)]^2} \quad \text{for } p^0 > \mu \tag{17}$$

$$k_{F,p}(\vec{p}) = [3\pi^2\rho_p(\vec{p})]^{1/3} \;\; k_{F,n}(\vec{r}) = [3\pi^2\rho_n(\vec{r})]^{1/3} \tag{18}$$

where for simplicity Σ is now $\bar{u}\Sigma u$ which is independent of spin.

By means of this new nucleon propagator the modifications introduced by our relativistic formalism, described in detail in ref. [23], are rather intuitive, easy to employ and can be summarized as:

i) The normalization of the spectral function which ensures the proper normalizations of the charge (or baryonic charge) of a nucleus is exactly the same as in eq.(9). However, the spectral function of eq.(12) is now replaced by eq. (17)

ii) On the other hand the structure function $F_{2A}(x)$ of eq.(8) is replaced by

$$F_{2A}(x) = 4\int d^3r \int \frac{d^3p}{(2\pi)^3}\frac{M}{E(\vec{p})}\int_{-\infty}^{\mu} d\omega\, S_h(\omega,p)\frac{x}{x_N}F_{2N}(x_N)\theta(x_N)\theta(1-x_N) \tag{19}$$

where the relativistic factor $\frac{M}{E(\vec{p})}$ plays the role of a Lorentz contraction factor, appearing in the probability per unit time of electron collision with the nucleon, and which remains in the formula of the nuclear cross section because one divides the sum of all probabilities by a unique electron flux, the one of the electron with respect to the CM of the nucleus.

The questions of normalization and conservation of baryonic number, which have been the subject of much attention [2], are discussed in detail in [23].

There are other terms which would be included in a covariant formalism of the (e,e') reaction and do not appear in our formalism. These are terms

which have a negative energy state coupled to the hadronization vertex, as shown in fig. 3. Once again such terms are reduced by the large energy denominator of the negative energy state. Only in cases when one uses an operator which magnifies the $N\bar{N}$ coupling with respect to the NN, as in the case of the axial charge, such terms can be relevant [26], although more accurate nonperturbative calculations find smaller results [27]. With the use of scalar potentials Σ^s smaller than the typical ones in the Walecka model when one imposes constraints from information in the negative energy sector, as done in [28], terms like in fig. 3 would be of the order of 10-15 % if one has an operator like in the axial charge, $\gamma^0\gamma_5$, but much smaller than this if electromagnetic current operators are used [27].

Furthermore, in as much as one assumes that the structure functions for the positive or negative energy states are the same and one uses a nucleon spectral function which conserves the baryonic number, one would be including the strength of these pieces into the scheme which we follow, up to small differences coming from different medium corrections to the positive and negative energy states. Estimates based on the findings of [27] would put the difference between this covariant scheme and ours at the level of 1-2% in the EMC region and probably a few percent in the $x > 1$ region that we explore.

In practical terms our scheme respects special relativity in the positive energy sector and amounts to using free $u_r(\vec{p})$ spinor in the evaluation of the matrix elements of the $\gamma^* N \to X$ process while keeping the proper energy and momentum balance in the δ function of conservation of fourmomentum, with the ω, p distribution of the occupied nucleon given by the spectral function and the energy and momentum of the final states in X being those of their asymptotic states. This is in fact the most standard method in the study of many nuclear processes involving scattering or decay. The aproximations which we have done here, sacrificing covariance in a controled way, lead us to this calculational scheme where everything is defined. Covariant formalisms like those used in [29, 30] generate some off shell dependence in the hadronic tensor, which are accounted for in terms of new structure functions for which there is no empirical information, so several different assumptions are made in [29, 30] which produce moderate changes in the EMC results.

Our relativistic corrections thus stem from the consideration of special relativity in the positive energy sector, although, as we discussed, it accounts in an approximate way for the contributions involving negative energy states, which are small anyway.

We will show results both with the relativistic and non-relativistic formalism. The relativistic corrections are found to be relevant in the region of $x > 1$, particularly at large values of x.

It is easy to see qualitatively why eq.(8) or eq.(19) lead to a non-vanishing structure function for $x > 1$. The nucleon structure function appears with argument x_N in this equation and in the Bjorken limit one has

$$x_N = \frac{x_N}{x} x = \frac{M}{\omega - p_z} x \tag{20}$$

For certain combinations of ω and p_z one can obtain values of $x_N < 1$ even if $x > 1$. Since both ω and p_z appear in eq.(20) it is very important to take into account the correlations between ω and p provided by the spectral function $S_h(\omega, p)$, and one sees that approximations which neglect these correlations are bound to provide unrealistic results.

3 The nucleon spectral function in nuclear matter and finite nuclei

We have used three different approaches to evaluate the spectral function. The first one is a semiphenomenological one relating the spectral function of nuclear matter to the experimental cross section for NN scattering. The second approach is microscopic in the sense that the spectral function for nuclear matter is derived from a many-body calculation employing a realistic One-Boson-Exchange model for the NN interaction. In the third model we avoid the local density approximation and evaluate the spectral function $\mathcal{S}_h$ directly for finite nuclei. We briefly describe these models below.

3.1 Semiphenomenological approach

This model is described in detail in ref. [31]. It evaluates $Im\Sigma(\omega, p)$ from a second order diagram and uses the fact that ladder diagrams evaluated from the NN potential lead to the NN t matrix. Pauli blocking corrections are taken into account in the explicit diagram evaluated and $|t|^2$, which appears in the evaluation of $Im\Sigma$, is written in terms of the experimental NN cross section. Polarization effects from the RPA iteration of ph and Δh excitations are also taken into account. The real part of the selfenergy is obtained via a dispersion relation and the Fock term from pion exchange is also included. Hartree terms, which require the explicit knowledge of a potential, are missing in the approach but these are terms independent of energy and momentum. The nucleon properties evaluated in [31] as a function of $\omega - \mu$ compare favourably with those of more microscopic evaluations [32, 33]. In order to complete the model and obtain absolute values for $Re\Sigma$, another phenomenological piece is added here. This Hartree contribution is assumed to be proportional to ρ and its value is adjusted, in order to fit the empirical value of the binding energy per nucleon in each particular nucleus. For this purpose we recall the sum rule for the binding energy per nucleon [34]

$$|\varepsilon_A| = -\frac{1}{2}\left(< E - M > + \frac{A-1}{A-2} < T > \right) \tag{21}$$

and we evaluate $< T >$ and $< E >$ as

$$< T >= \frac{4}{A}\int d^3r \int \frac{d^3p}{(2\pi)^3}(E(\vec{p}) - M)\int_{-\infty}^{\mu} S_h(\omega, p)d\omega$$

$$< E >= \frac{4}{A}\int d^3r \int \frac{d^3p}{(2\pi)^3}\int_{-\infty}^{\mu} S_h(\omega, p)\omega\, d\omega \qquad (22)$$

By means of this, one takes also into account empirically contributions from terms like in fig. 2e, which are in principle small, and even if they are of ρ^2 type would not differ appreciably from a $\rho\,\rho_{eff}$ form, with ρ_{eff} an effective average nuclear density.

The evaluation of $Im\Sigma(\omega, p)$ was done nonrelativistically in [31]. For consistency with the relativistic formalism used here we should have kept the factors $\frac{M}{E}$ in the nucleon propagators evaluating $Im\Sigma(\omega, p)$ in ref. [31]. However, the range of momenta in the loop integrals in $Im\Sigma(\omega, p)$ is quite limited and they would modify the values of $Im\Sigma(\omega, p)$ by less than 10%. By means of the explicit calculations carried out here we have observed that an increase of 10 % in $Im\Sigma(\omega, k)$ leads to increases of $F_{2A}(x)$ of the order 2 % at $0 < x < 0.6$ and always below the 10 % level for large x, hence we have continued to use the same $Im\Sigma(\omega, p)$ as obtained in ref. [31].

3.2 Microscopic approach in nuclear matter

The spectral function of nuclear matter which has been used in this second approach has been evaluated using the techniques described in ref. [35]. The starting point of this many-body calculation is a Brueckner-Hartree-Fock (BHF) calculation of nuclear matter considering the realistic One-Boson-Exchange (OBE) potential B as defined in [36] for the NN interaction. The G-matrix resulting from this BHF calculation as well as the BHF single-particle spectrum $\epsilon_{BHF}(p)$ are used to define the nucleon self-energy including all terms up to second order in G. The single-particle Green's function $g(p, \omega)$ is derived from a solution of the Dyson equation

$$g(p, \omega) = g^{(BHF)}(p, \omega) + g^{(BHF)}(p, \omega)\left[\Sigma^{(2)}(p, \omega)\right] g(p, \omega) \qquad (23)$$

Here $\Sigma^{(2)}$ is the contributions to the self-energy in second order. The single-particle Green's function in the BHF approximation is given by

$$g^{(BHF)}(p, \omega) = \frac{\Theta(k_F - p)}{\omega - \epsilon_p - i\eta} + \frac{\Theta(p - k_F)}{\omega - \epsilon_p + i\eta}\,, \qquad (24)$$

where k_F denotes the Fermi momentum of nuclear matter at the density under consideration. The term with $\Sigma^{(2)}$ in eq. (23) contains a contribution with intermediate particle-particle states, which is taken into account already in the BHF aproximation. This doublecounting is removed as described in [35]. The spectral function $S_h(\omega, p)$ can then be calculated from the imaginary part of the single-particle Green's function by

$$S_h(\omega, p) = \frac{1}{\pi} Im\, g(p, \omega) \tag{25}$$

This calculation yields a Fermi energy μ depending on the density of nuclear matter. The energy variable ω is defined with respect to this Fermi energy. In the local density approximation for the spectral function discussed above, the empirical Fermi energy of the finite nucleus has been chosen to be the reference point for the energy variable ω.

3.3 Microscopic approach for finite nuclei

The spectral function can be calculated directly for finite nuclei using the procedure described and applied to ^{16}O in ref. [37]. For nuclei with spherical symmetry the self-energy is evaluated in a partial wave basis, $\Sigma_{lj}(p, p')$, assuming that orbital angular momentum l and total angular momentum j are conserved quantum numbers. As discussed above, the total self-energy is decomposed in a BHF part and terms of second order in the Brueckner G-matrix. The corresponding single-particle Green's function can be evaluated by solving a Dyson equation of the form

$$\begin{aligned} g_{l,j}(p, p'; \omega) = g^{(BHF)}_{l,j}(p, p'; \omega) + \quad & \int dk_1 \int dk_2 \; g^{(BHF)}_{l,j}(p, k_1; \omega) \\ & \times \left[\Sigma^{(2)}_{l,j}(k_1, k_2; \omega)\right] g_{l,j}(k_2, p'; \omega) \end{aligned} \tag{26}$$

The spectral function for the various partial waves is then obtained from the imaginary part of the Green's function $g_{l,j}(p, p; \omega)$ applying eq.(25). A problem of this partial wave expansion for the momentum distribution is related to the fact that non-negligible contributions are obtained at large momenta and energies in high partial waves. Therefore we prefer to apply an approach which has been introduced and discussed in ref. [35]. In this approximation one splits the spectral function, for nuclear matter as well as for finite nuclei, into a quasiparticle contribution describing the contribution to the spectral function around the quasiparticle pole and a background contribution which contains the information about the spectral function at energies away from the respective quasiparticle pole. For finite nuclei a quasiparticle pole contribution is only observed for those partial waves, which are occupied in the HF or independent particle model. Therefore the sum on partial waves in

$$S^{QP}(\omega, p) = \sum_{l,j} 2(2j+1) n_{l,j} \delta(\omega - \epsilon^{QP}_{l,j}) |\Phi_{l,j}(p)|^2 \tag{27}$$

is restricted to l=0 and 1 in our example of ^{16}O. In this equation $\epsilon^{QP}_{l,j}$ stands for the energy of the quasiparticle pole, $\Phi_{l,j}(p)$ for the corresponding single-particle wave function in momentum space and $n_{l,j}$ for the occupation probability for this pole. This quasiparticle pole contribution is supplemented by

the background contribution calculated in a local density approximation from the background contribution in nuclear matter

$$S_{h,A}(\omega,p) = S^{QP}(\omega,p) + 4\int d^3r S_h^B(\omega,p;\rho(r)) \tag{28}$$

where S_h^B stands for the background contribution of the spectral function calculated in nuclear matter at the local density $\rho(r)$. Care is taken that the whole spectral function is normalized such that

$$\int \frac{d^3p}{(2\pi)^3}\int_{-\infty}^{\mu} d\omega S_{h,A}(\omega,p) = A \tag{29}$$

with A the total number of nucleons.

3.4 Approximations to be avoided

If no reliable model for the spectral function for nucleons in nuclear matter is available, one may be tempted to use certain approximations. One of such approximations, which has frequently been used [12–14] is to ignore the special correlations between momentum and energies of nucleons provided by the spectral function and simply use the energy-integrated spectral function, which is the momentum distribution. We are going to discuss three different approximations and try to explore their reliability by comparing with the results obtained in the more sophisticated models for the spectral function discussed above. Although discussions around different approximations to the nuclear wave functions, and other different approximations, have been common in the past [2, 4, 7, 38], the comparison of different approximations to the results obtained using spectral functions has not been exploited, particularly in the region of $x > 1$ which we study here.

a) The uncorrelated Fermi sea distribution.
This is the simplest approximation, which is usually very accurate, except of course in processes which test the momentum distribution at momenta which are large compared to the Fermi momentum, as is the case in the present problem. In this approximation the spectral function within the local density approximation is assumed to have the form

$$S_h^{UFS}(\omega,p;\rho) = n_{FS}(\vec{p})\delta(\omega - E(\vec{p}) - \Sigma) \tag{30}$$

with an occupation probability of

$$n_{FS}(\vec{p}) = \begin{cases} 1 & \text{if } |\vec{p}| < p_F(r) \\ 0 & \text{if } |\vec{p}| > p_F(r) \end{cases} \tag{31}$$

with a local Fermi momentum $p_F(r)$ which is related to the local density $\rho(r)$ by

$$p_F(r) \equiv (\frac{3\pi^2\rho(r)}{2})^{1/3} \tag{32}$$

and an expression for the local single-particle potential

$$\Sigma \equiv \Sigma(r) = V_{TF}(r) + D\rho(r) \tag{33}$$

where $V_{TF}(r)$ is the Thomas Fermi potential, $-p_F^2(r)/2M$ and D a phenomenological constant fitted to reproduce the binding energy per nucleon in the nucleus, as done in section 3.1.

b) Use of the momentum distribution of the correlated Fermi sea.

Since large momentum components are needed to generate $F_{2A}(x)$ at $x > 1$, one is tempted to use the realistic momentum distribution of the nucleus as a way to improve on this approximation. This means that we assume an expression for the spectral function S_h^{MD} like in eq.(30) but replace the momentum distribution of the free Fermi gas n_{FS} by the momentum distribution of the interacting Fermi gas

$$n_I(\vec{p}) = \int_{-\infty}^{\mu} S_h(\omega, p) d\omega \tag{34}$$

where we have used the spectral function of nuclear matter discussed above to calculate n_I. Note, however, that the energy-momentum relation is still determined by the δ-function in (30), with Σ defined with the same prescription as in the subsection above, eq. (33).

c) Use of the correlated momentum distribution and the corresponding mean value for the energy.

Finally we want to consider an approximation in which we assume again a definite relation between momentum and energy of a nucleon in the hole spectral function

$$S_h^{MED}(\omega, p; \rho) = n_I(\vec{p})\delta(\omega - < \omega(\vec{p}) >) \tag{35}$$

but determine the momentum distribution n_I (see eq.(34)) as well as the mean value of the energy for a given momentum

$$< \omega(\vec{p}) > = \frac{\int_{-\infty}^{\mu} S_h(\omega, p)\omega d\omega}{\int_{-\infty}^{\mu} S_h(\omega, p) d\omega} \tag{36}$$

from the complete spectral function for nuclear matter discussed above.

4 Results and discussion

In a first step we want to compare the two approaches to determine the spectral function for nuclear matter, which we describe in sections 3.1 and 3.2 and which

we are going to employ for the calculation of the structure function. For that purpose we present in Fig. 4 the momentum distribution $n_I(p)$ (see eq.(34)) calculated at the empirical saturation density, $\rho = \rho_0$, of nuclear matter.

The momentum distributions obtained by these two very different methods are very similar. At small values of p the microscopic approach of [35] provides an occupation number of the order of 3 % bigger than the semiphenomenological one [31]. For momenta above the Fermi momentum the distributions are also similar although for momenta around two times the Fermi momentum ($\sim 550\, MeV/c$) the differences become more appreciable. The semiphenomenological approach provides a little less strength below the Fermi momentum, which is then redistributed to larger momenta where $n_I(\vec{p})$ is larger than in the microscopic approach. The precise values of $n_I(\vec{p})$ calculated in a microscopic many-body theory, depend on the model of the NN interaction which is considered and the method which is used to determine the effects of correlations. For instance in the self-consistent Green's function approach of ref. [33], using the Reid soft-core potential, the occupation number for momenta below k_F is around 0.85, smaller than in both the approaches considered here. This demonstrates that the semiphenomenological approach provides a result which is in agreement with the microscopic calculations within the uncertainties of the microscopic approach caused by the approximation in the many-body theory as well as NN interaction. The differences found in $n_I(\vec{p})$ in the two approaches discussed have little repercussion in the values of $F_{2A}(x)$, which come very close to each other in the two approaches, as we shall see below.

As a second quantity characterizing the bulk properties of the spectral functions calculated by these two methods, we show in Fig. 5 the mean value for the energy as a function of $\vec{p}$ calculated according to eq.(36) at the nuclear density ρ_0. Fig. 5 shows in a qualitative way that there is an important correlation between the momenta and the mean value of the energy for the bound nucleons. The absolute value of this mean energy $| < \omega(\vec{p}) - M > |$ decreases as a function of momentum with increasing momenta for momenta below the Fermi momentum. This momentum dependence is mainly due to the momentum of the quasiparticle peak, which is approaching the Fermi energy for $p \to p_F$. There is no quasiparticle contribution to the hole-spectral function S_h for momenta larger than the Fermi momentum p_F. Therefore at these momenta, the mean value is determined only from the background contribution. The coupling to 2 hole-1 particle and more complicated configurations with total momenta p, described by these background terms yields a mean value of $< \omega - M >$, which decreases with increasing momentum. From this figure it is evident, however, that the energy-momentum relation obtained from a realistic spectral function is quite different from the simple relation used in eqs. (30), (33), which provides a dispersion relation which is always an increasing function with increasing momentum.

The values obtained for $| < \omega(\vec{p}) > |$ in the two approaches discussed in sections 3.1, 3.2 are very similar, with differences of the order of 10 % at most.

This is another indication that the basic features of the spectral function are not very sensitive to the method used in the evaluation and that also the semiphenomenological approach yields quite a reliable result.

In Fig. 6 we show the results for $F_{2A}(x)$ calculated with the three different spectral functions introduced in sections 3.1 to 3.3, for the case of ^{16}O. The density distributions $\rho(r)$ for ^{16}O and the other nuclei, which are required to apply the local density approximation, are taken from refs. [39, 40]. Since the microscopic nuclear matter and finite nuclei approaches are nonrelativistic, we have also taken the nonrelativistic version of the semiphenomenological approach, for comparison, omitting all the $\frac{M}{E(p)}$ factors in eqs. (17), (19). The experimental values for $F_{2N}(x_N)$ are taken from ref. [41]. The results obtained with the two spectral functions of nuclear matter (solid line and dashed line) are rather similar. At $x \simeq 1$ the microscopic spectral function provides results about 20 % higher than the semiphenomenological one. At values of $x \simeq 1.22$ the two approaches coincide and for $x \simeq 1.5$, where the structure function has decreased three orders of magnitude with respect to the value at $x = 1$, the semiphenomenological approach provides values of F_{2A} about 40 % larger than the microscopic one. This reflects the fact that the former model provides a larger probability for the momentum distribution at high momenta than the latter one, as seen in Fig. 4.

The results for the structure function obtained with the spectral function of eq.(28) evaluated directly for the finite nucleus are represented by the dot-dashed line in Fig. 6. They should be compared with those displayed by the solid line since the background contribution to eq.(28) is obtained from the same nuclear matter result. These two results can hardly be separated on the logarithmic scale of the figure. We observe that at $x \simeq 1$ the results with the spectral function of the finite nucleus are about 8 % bigger than with the nuclear matter approach. The differences become smaller as x increases and for values of $x \simeq 1.5$ the two approaches give the same results. This latter fact is telling us that at large values of x one is getting practically all contributions from the background part of the spectral function and none from the quasiparticle part. The comparison of these two curves also tells us that the use of the nuclear matter spectral functions, together with the local density approximation, is an excellent tool to evaluate $F_{2A}(x)$. If one compares the results at values of x studied in the EMC effect, $0 < x < 0.6$, the differences among the three calculations are of the order of 3 %.

In Fig. 7 we show results obtained with the semiphenomenological approach using the relativistic and nonrelativistic formalisms. The trend of the results is similar, however, the relativistic corrections induce a reduction of 25 % around $x = 1$ and roughly reduce the structure function F_{2A} to one half of the non relativistic results at $x \simeq 1.5$. The relativistic effects are significant in the sense that they are bigger than the differences found between various nonrelativistic approaches, which reflect the uncertainties in the treatment of correlations.

Results obtained for $F_{2A}(x)$ using the different approximations discussed in section 3.4 are displayed in Fig. 8. The first one, which originates from the assumption of an uncorrelated Fermi sea, eq. (30), is represented by the dot-dashed line. We can see that at $x \simeq 1$ it already provides a structure function of around a factor two smaller than the one obtained with the proper spectral function (short dashed-line). However, as one moves to higher x, the discrepancies get bigger and at values of $x \simeq 1.2$ the uncorrelated Fermi sea gives already values for the structure function which are about two orders of magnitude smaller than the correct ones. It is clear that one is exploring the region of large momenta, above the Fermi momentum, which are not accounted for by the uncorrelated Fermi sea.

Another approximation corresponds to using the realistic momentum distribution $n_I(\vec{p})$ of eq. (34) and associating an energy to each $\vec{p}$ given by its kinetic energy plus a potential, eq. (33). The results (solid line) are outrageously wrong. This demonstrates that the naive use of a momentum distribution, although calculated in a realistic way, may lead to results which are worse than those obtained for an uncorrelated system, if one does not treat the energy-momentum correlation properly. As we have discussed already in Fig. 5, the mean value of the energy $< \omega(\vec{p}) >$ decreases above the Fermi momentum with increasing momenta. On the other hand, the energy associated to $\vec{p}$ in eq. (30) grows like the kinetic energy as $|\vec{p}|$ increases. The discrepancies with the correct results are about a factor three at $x \simeq 1$ and three orders of magnitude at $x \simeq 1.5$, providing a gross overestimate of the results for $F_{2A}(x)$. The same gross overestimate found here for this approximation was also found in ref. [15] in connection with the mesonic Lambda decay in nuclei.

In view of the deficiencies of the previous approximations and the reasons for it, one might think that the results should be improved by replacing the kinetic plus potential energy, eq. (30), by the mean value of $< \omega(\vec{p}) >$ calculated from the spectral function (see eq.(36). This is indeed the case (see curve with long dashes in Fig. 8), although the discrepancies with the exact results are still large enough to discourage this approximation too. We can see in Fig. 8 that at values of $x \simeq 1$ (and also in the EMC region below) the approximation turns out to be quite good. However, for values of $x \simeq 1.3$ and above the discrepancies with the correct results are already as big as one order of magnitude or more.

The results discussed here stress the importance of using the spectral function to evaluate $F_{2A}(x)$ since all the information contained in it, correlating energies and momenta, is very important, particularly at large x. We showed that some schemes which use only a partial information from the spectral function lead to rather inaccurate results and should thus be avoided.

Finally in Fig. 9 we show results obtained for different nuclei. They are calculated at $Q^2 = 5\ GeV^2$. We can see that $F_{2A}(x)/A$ is very similar for the different nuclei. We have taken nuclei with $N = Z$ or close by, to be able to use a unique Fermi sea for protons and neutrons as done in symmetric nuclear matter. For heavier nuclei with $N \neq Z$ the results obtained here could

be easily extended by dealing with two different Fermi seas, but this would require the extension of the work of ref. [31] to non symmetric nuclear matter. We do not expect, however, any special effects apart from those exposed here.

When evaluating absolute values of nuclear structure function, not ratios to the nucleon or the deuteron, it is very important to take into account the Q^2 dependence of the structure function. This is particularly true for values of $Q^2 \simeq 1 - 10\ GeV^2$, but even at $Q^2 \simeq 100\ GeV^2$ and above, where there is approximate Bjorken scaling, the Q^2 dependence is weak but one still has to consider it if one wants to make accurate predictions.

For the Q^2 dependence of the nucleon structure function we have taken the parametrizations given in ref. [42].

It is interesting to compare our results with the scarce experimental data available. Our results refer exclusively to the deep inelastic contribution to electron nucleus scattering. The quasielastic contribution (where only one nucleon is knocked out in the first step $eN \rightarrow e'N$) is not taken into account in our formalism. At low values of Q^2 and $x \geq 1$, the quasielastic contribution is dominant [19] and one has to go to values of $Q^2 > 20\ GeV^2$ to have a dominance of the deep inelastic contribution [17]. For this reason we compare our results with measurements done at $Q^2 = 61, 85$ and $150\ GeV^2$ in ref. [43], which improve the preliminary results reported in ref. [44] where much larger values were obtained.

The results can be seen in fig. 10. The three theoretical curves correspond to each one of the values of Q^2 and the results decrease as a function of increasing Q^2. The agreement with the data is qualitative. The slope as a function of x seems well reproduce but the theoretical results are in average 40 % higher than experiment up to $x = 1.05$. At $x = 1.15$ and 1.3 there are only upper bounds which are compatible with our predictions.

Experimental results at $Q^2 < 5\ GeV^2$ have however, a large contamination of quasielastic contribution [17–19]. This is reflected by the large dispersion of the results as a function of Q^2 [45] and in the approximate y scaling of these results, which is characteristic of the quasielastic collisions. Nevertheless, we have also evaluated the deep inelastic contribution correspondieng to the results in [45] with largest values of Q^2. We evaluate the structure function corresponding to the lowest curve in fig. 1 of ref. [45]. This corresponds to different values of Q^2 for each value of x since the data correspond to electron scattering with fixed initial electron energy ($E_e = 3.595\ GeV$), fixed scattering angle, $\theta = 39^0$ and variable final electron energy. We show the results in fig. 11. The values of Q^2 increase with increasing x. At $x = 1\,, Q^2 = 3.11\ GeV^2$ and at $x = 1.25\,, Q^2 = 3.42$. We can see that our results lie below the experimental data, particularly at large values of x. However, one can observe a tendency to be in agreement with the data at values of $x < 0.8$ if one extrapolates the data smoothly. In fact in fig. 1 of ref. [45] we see a confluence of the data for different values of Q^2 in the region of $x = 0.4 - 0.6$ with values which agree with our results of fig. 11. This would be in agreement with the conclusions reached in [45] where the large dispersion of the results as a function of Q^2

for large values of x indicates the dominance of the quasielastic contribution, while the tendency to stabilize the results at values of $x < 0.8$ indicate that this region of x is dominated by the deep inelastic contribution. In such case our results should be comparable to the data and this is indeed the case.

5 Conclusions

We have evaluated the nuclear structure function $F_{2A}(x)$ at values of x bigger than unity, especially in the range $1 < x < 1.5$ where the values obtained are well within measurable range. For this purpose we have used sophisticated nuclear spectral functions which account for nuclear correlations and relativistic effects. The structure function decreases three orders of magnitude from $x = 1$ to $x = 1.5$.

The strength of $F_{2A}(x)$ in that range of x is tied to the components of the nuclear wave function with nucleons of large momenta. These components are due to the two-nucleon correlations originating from realistic NN interactions. The momentum distribution of nucleons in the nuclear many-body system, however, is strongly correlated with the energy distribution of these nucleons. These are dynamical effects which go beyond the shell model picture of the nucleus and which are taken into account in terms of the nucleon spectral functions. The results for $F_{2A}(x)$ are very sensitive to the correlations between ω and p, to the extreme that usual approximations made in calculations of the EMC effect fail badly in the region of $x > 1$. In particular, at $x \simeq 1.5$ the quasiparticle bound states (the occupied states of the shell model), which are only partly occupied in an interacting nucleus, give a negligible contribution to $F_{2A}(x)$ and all the strength comes from the background part of the spectral function.

We have discussed in detail the results obtained with several approximations which use only rough spectral functions or partial information from realistic ones, and which are often used. We showed that in this region of x none of them can be taken as a substitute of the calculation using the whole information of the spectral function.

In order to quantify the intrinsic theoretical uncertainties of the results we used two different models for the spectral function evaluated in infinite nuclear matter and $F_{2A}(x)$ for nuclei was calculated using the local density approximation. A version of the spectral function for finite nuclei was used also for ^{16}O. The differences between the models were small, of the order of 10-30 % depending on the region of x. We also found that the use of the local density approximation was an excellent tool, providing results very close to those obtained by direct evaluation for the finite nucleus.

Relativistic effects were checked and found to be important. They reduce the results for $F_{2A}(x)$ obtained with the nonrelativistic approximation by amounts ranging from 25 % at $x \simeq 1$ to nearly a factor two at $x \simeq 1.5$.

On the other hand we have evaluated $F_{2A}(x)$ for different nuclei and find

that $F_{2A}(x)/A$ becomes very similar for $N = Z$ nuclei from ^{40}Ca on.

The experimental results at $x > 1$ are scarce, particularly at large values of Q^2. We compared our results with available data at $Q^2 = 61, 85, 150\ GeV^2$ and found our results about 40% higher than experiment, although the fall down with x was well reproduced. At values of Q^2 significantly smaller, $Q^2 < 4\ GeV^2$, we found that our results for $x > 1$ where much smaller than the experimental data, which was in agreement with theoretical and experimental findings that this region is dominated by quasielastic scattering. At lower values of x, around $x = 0.4 - 0.6$ our results matched the experimental data, in agreement with the theoretical and experimental findings that this region is dominated by the deep inelastic contribution.

The present investigation and the importance of the nucleon spectral function for the precise determination of $F_{2A}(x)$ is telling us that measurements of this quantity for different values of x and a wide range of nuclei would provide important information on the components of the nuclear wave function at large momenta and energies and the strong correlations between momenta and energy. This information would be very important as a test of the many body theories which are employed for the determination of the spectral function and would unveil interesting details on nuclear correlations, which complement our knowledge of nuclear structure beyond the basic information contained in the shell model wave functions.

Acknowledgments:

We would like to thank discussions with D.B. Day, J. S. McCarthy and R. Minehart concerning their experiment [45] and with G.I. Smirnov concerning the experiment of ref. [43]. Discussions with F. Gross and S. Liuti on theoretical issues are equally appreciated.

One of us, E.O. wants to thank the Humbold Foundation who supported his stay at Tübingen. P.F. and E.M. wish to thank the financial support of the Human Capital and Mobility program of the EU, contract no. CHRX-CT 93-0323. The work is partly supported by CICYT contract no. AEN 93-1205.

Figure Captions:

Fig. 1: a) Feynman diagram for deep inelastic electron-nucleon scattering and, b) electron selfenergy diagram associated to it.

Fig. 2: a,b,c,d) Feynman diagrams of the Dyson series in the evaluation of the nucleon propagator including only intermedite positive energy states. e) Feynman diagram of the Dyson series with a negative energy intermediate state. f) Higher order terms in the Dyson series originated from the selfenergy

term of diagrame and its iteration through positive energy intermediate states.

Fig. 3. Feynman diagram for deep inelastic electron scattering with an interating nucleon, through the coupling of the photon to the negative energy components.

Fig. 4: Momentum distributions at $\rho = \rho_0$. Solid line: microscopic model of [35]; dashed line: semiphenomenological model [31].

Fig. 5: Mean value of the energy of nucleons as a function of $\vec{p}$, from eq. (36), at $\rho = \rho_0$. Solid line: microscopic model [35]; dashed line: semiphenomenological model [31].

Fig. 6: Results obtained for the structure function of ^{16}O. Solid line: microscopic nuclear matter model [35]; dot-dashed line: microscopic finite nuclei model eq.(23); dashed line: nonrelativistic semiphenomenological model [31].

Fig. 7: Results obtained for the structure function of ^{16}O using the semiphenomenological model [31]. Solid line: nonrelativistic formalism; dashed line: relativistic formalism.

Fig. 8: Results obtained for the structure function of ^{16}O using different approximations. Dot-dashed line: uncorrelated Fermi sea, eq. (25); solid line: momentum distribution of the correlated Fermi sea, eq. (29); long dashed line: momentum distribution of the correlated Fermi sea and average energy $< \omega(\vec{p}) >$, eq. (30); short dashed line: spectral function, eq. (13). $Q^2 = 5\ GeV^2$.

Fig. 9: Results obtained for the structure function per nucleon for different nuclei. Solid line: ^{40}Ca; short dashed line: ^{56}Fe; dot-long dashed line: ^{12}C; dot-short dashed line: ^{16}O; long dashed line: ^{6}Li. All results are obtained using the relativistic version of the spectral function, eq. (13). $Q^2 = 5\ GeV^2$.

Fig. 10: Results for the structure function of ^{12}C at $Q^2 = 61, 85$ and $150\ GeV^2$ (solid, short-dashed and long dashed lines respectively). The data are from ref. [43] crosses for 61 GeV^2, squares for 85 GeV^2 and triangles for 150 GeV^2. The data for the two largest values of x are upper bounds.

Fig. 11: Results for the deep inelastic structure function of ^{56}Fe at different values of Q^2 around 3 GeV^2, see text, compared with experimental inclusive data results of [45]. The experimental data for values of $x > 1$ are dominated by the quasielastic contribution while for values of $x < 0.8$ the deep inelastic contribution dominates the reaction.

References

[1] E.M. Collaboration, J.J. Aubert al., Phys. Lett. B123 (1983) 275.

[2] L.L. Frankfurt and M.I. Strikman, Phys. Rep. 160 (1988) 236.

[3] R.P. Bickerstaff and A.W. Thomas, J. Phys. G15 (1989) 1523.

[4] A. B. Migdal, E.E. Saperstein, M.A. Troitskii and D.N. Voskresenskii, Phys. Rep. 192 (1990) 179.

[5] M. Arneodo, Phys. Rep. 240 (1994) 301.

[6] C.H. Llewellyn Smith, Phys. Lett. B128 (1983) 107.

[7] M. Ericson and A.W. Thomas, Phys. Lett. B128 (1983) 112.

[8] V. Sanjosé, V. Vento and S. Noguera, Nucl. Phys. A470 (1987) 509. P. González and V. Vento, Mod. Phys. Lett. A8 (1993) 1563.

[9] S.V. Akulinichev, S. A. Kulagin and G.M. Vagradov, Pis'ma Zh. Eksp. Teor. Fiz. 42 (1985) 105; JETP Lett. 42 (1985) 127; Phys. Lett. 158B (1985) 485.

[10] G. V. Dunne and A.W. Thomas, Phys. Rev. D33 (1986) 2061.

[11] S. V. Akulinichev and S. Shlomo, Phys. Rev. C33 (1986) 1551.

[12] A. Bodek and J.L. Ritchie, Phys. Rev. D23 (1981) 1070.

[13] H. Araseki and T. Fujita, Nucl. Phys. A439 (1985)681.

[14] K. Saito and T. Uchiyama, Z. Phys. A322 (1985) 299.

[15] P. Fernández de Córdoba and E. Oset, Nucl. Phys. A528 (1991) 736.

[16] C. Ciofi degli Atti and S. Liuti, Phys. Rev. C41 (1990) 1100.

[17] S. Liuti, Phys. Rev. C47 (1993) R1854.

[18] S. Simula, Few Body Systems Suppl. 8 (1995) 423.

[19] O. Benhar, A. Fabrocini, S. Fantoni and I. Sick, Phys. Lett. B343 (1995) 47.

[20] F. Gross and S. Liuti, Phys. Rev. C45 (1992) 1374.

[21] S. Liuti and F. Gross, Phys. Lett. B356 (1995) 157.

[22] L.L. Frankfurt and M.I. Strikman, Phys. Lett. B183 (1987) 254.

[23] E. Marco, P. Fernández de Córdoba and E. Oset, University of Valencia, preprint, nucl-th/9510060.

[24] C. Itzykson and J.B. Zuber, Quantum Field Theory (McGraw Hill, NY, 1980).

[25] B. D. Serot and J.D. Walecka, Adv. Nucl. Phys. 16 (1986) 1.

[26] M. Kirchbach, D.O. Riska and K. Tsushima, Nucl. Phys. A542 (1992) 616.

[27] A. Gil, M. Kleinmann, H. Müther and E. Oset, Nucl. Phys. A584 (1995) 621.

[28] J. A. Tjon and S.J. Wallace, Phys. Rev. C32 (1985) 267; C35 (1987) 280; C36 81987) 1085.

[29] W. Melnitchouk, A.W. Schreiber and A.W. Thomas, Phys. Rev. D49 (1994) 1183.

[30] S. A. Kulagin, G. Piller and W. Weise Phys. Rev. C50 (1994) 1154.

[31] P. Fernández de Córdoba and E. Oset, Phys. Rev. C46 (1992) 1697.

[32] S. Fantoni, B.L. Friman and V.R. Pandharipande, Nucl. Phys. A 399 (1983) 51; S. Fantoni and V. R. Pandharipande, Nucl. Phys. A427 (1984) 473.

[33] A. Ramos, A. Polls and W.H. Dickhoff, Nucl. Phys. A 503 (1989) 1.

[34] D.S. Koltun, Phys. Rev. C9 (1974) 484.

[35] H. Müther, G. Knehr and A. Polls, Phys. Rev. C., C52 (1995) 2955.

[36] R. Machleidt, Adv. Nucl. Phys. 19 (1989) 189.

[37] H. Müther, A. Polls and W. H. Dickhoff, Phys. Rev. C51 (1995) 3040.

[38] G. B. West, Phys. Lett. B37 (1971) 509.

[39] H. de Vries, C. W. de Jager and C. De Vries, At. Data and Nucl. Data Tables, 36 (1987) 495.

[40] G. C. Li, I. Sick, R. R. Whitney and M. R. Yearian, Nucl. Phys. A162 (1971) 583.

[41] J. J. Aubert et al., Phys. Lett. B114 (1982) 291.

[42] D.W. Duke and J.F. Owens, Phys. Rev. D30 (1984) 49.

[43] A. C. Benvenuti et al., Z. Phys. C63 (1994) 29.

[44] A. M. Baldin, Nucl. Phys. A434 (1985) 695c.

[45] B. W. Filippone et al., Phys. Rev. C45 (1992) 1582.

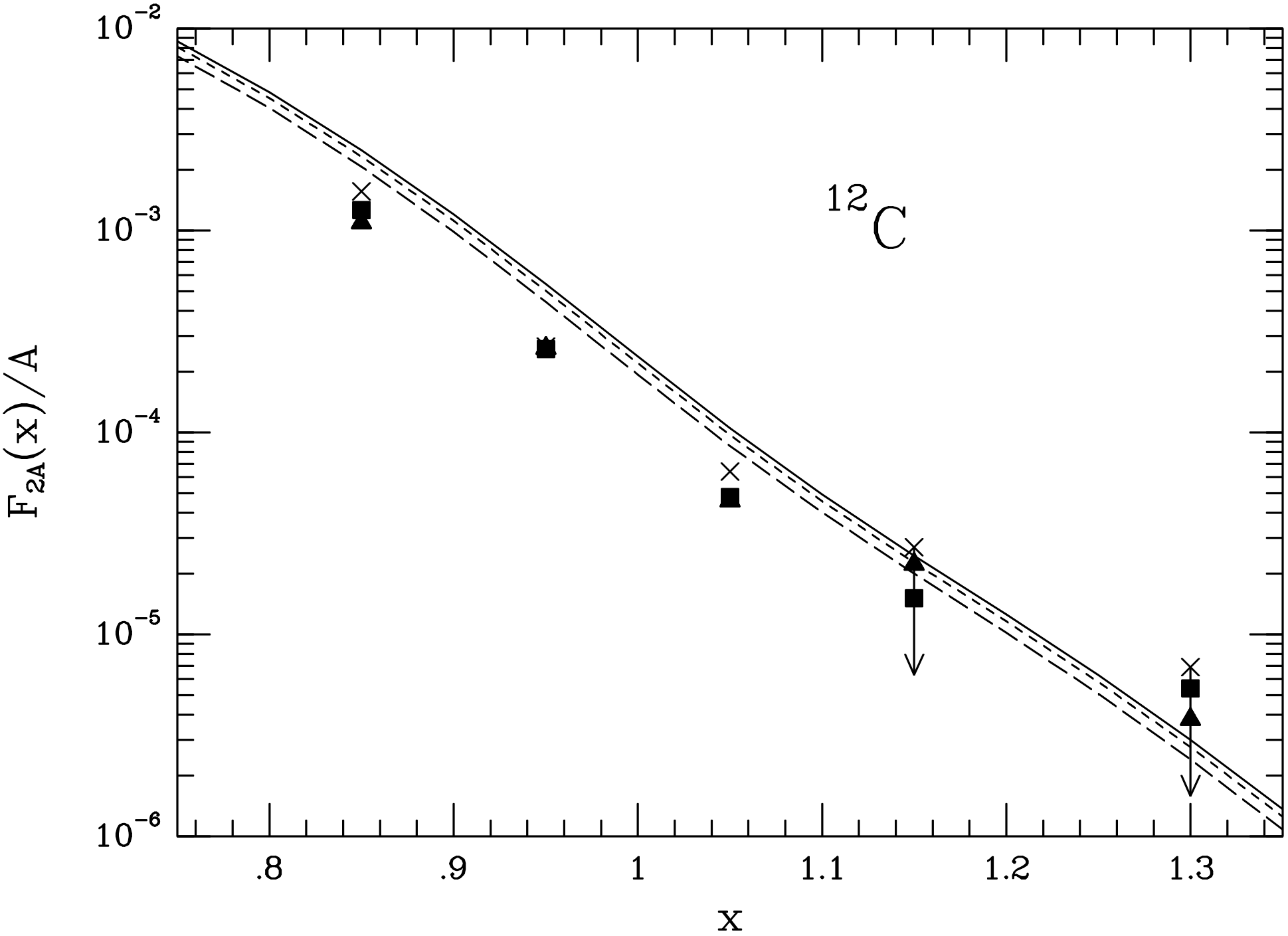
10^{-2}
10^{-3}
10^{-4}
10^{-5}
10^{-6}
$F_{2A}(x)/A$
^{12}C
.8
.9
1
1.1
1.2
1.3
x

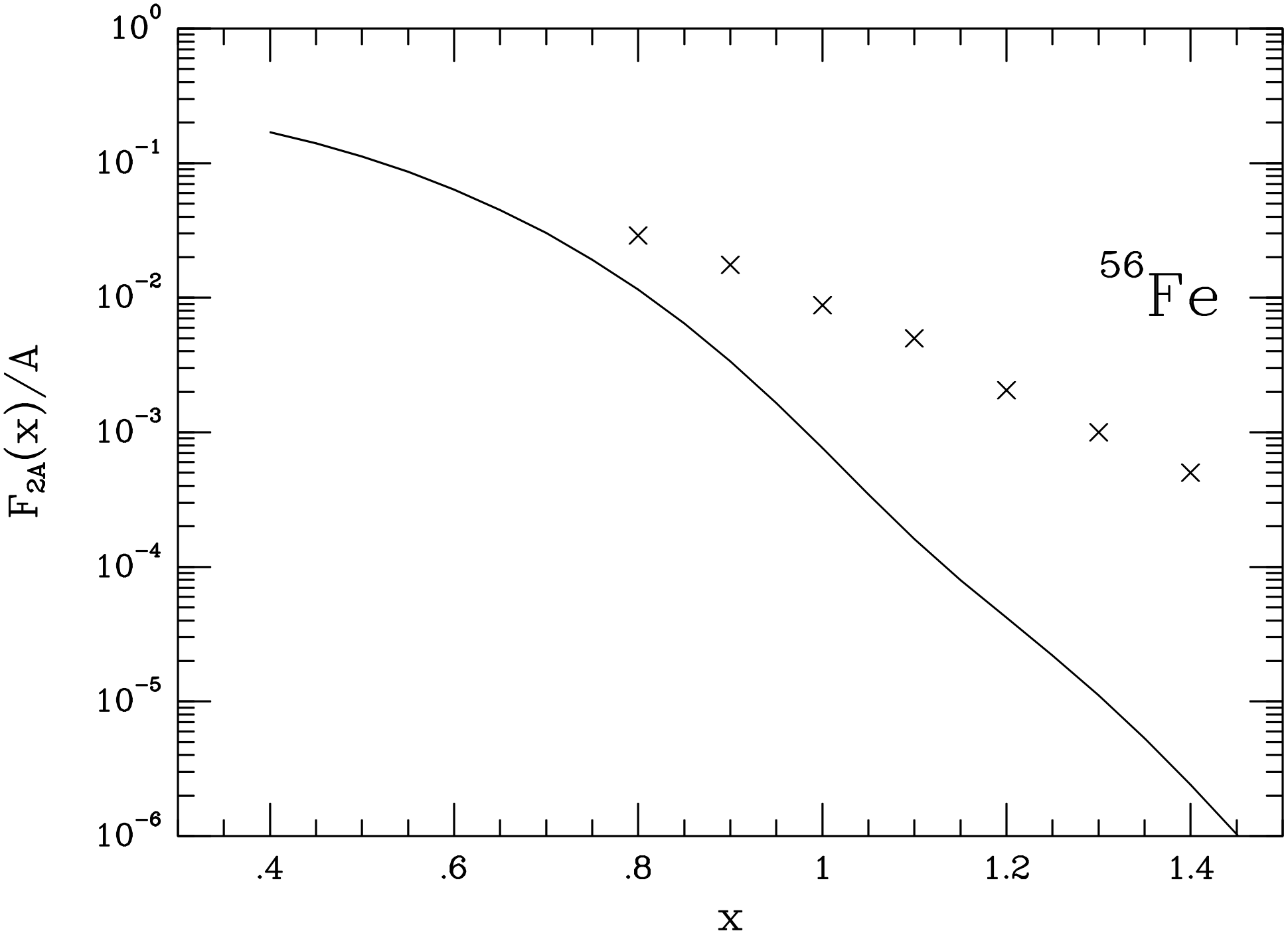
10^{0}
10^{-1}
10^{-2}
10^{-3}
10^{-4}
10^{-5}
10^{-6}
$F_{2A}(x)/A$
.4
.6
.8
1
1.2
1.4
x
^{56}Fe

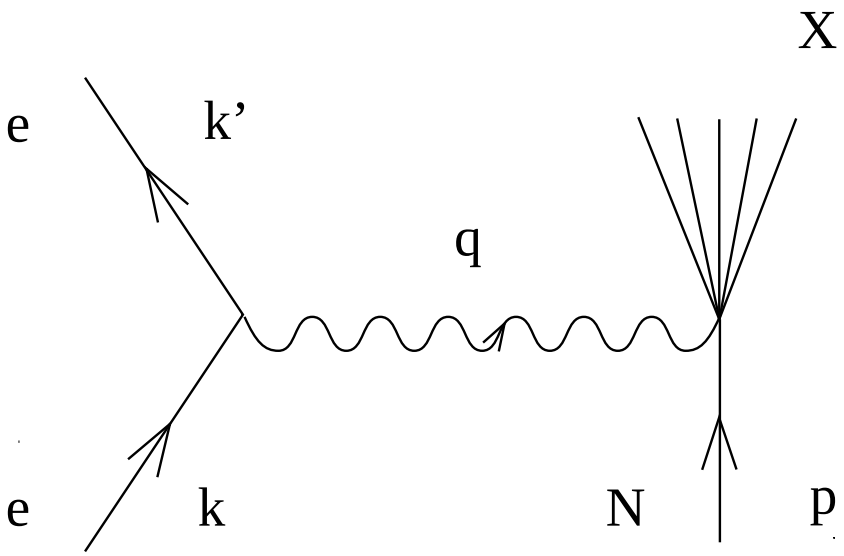

a)

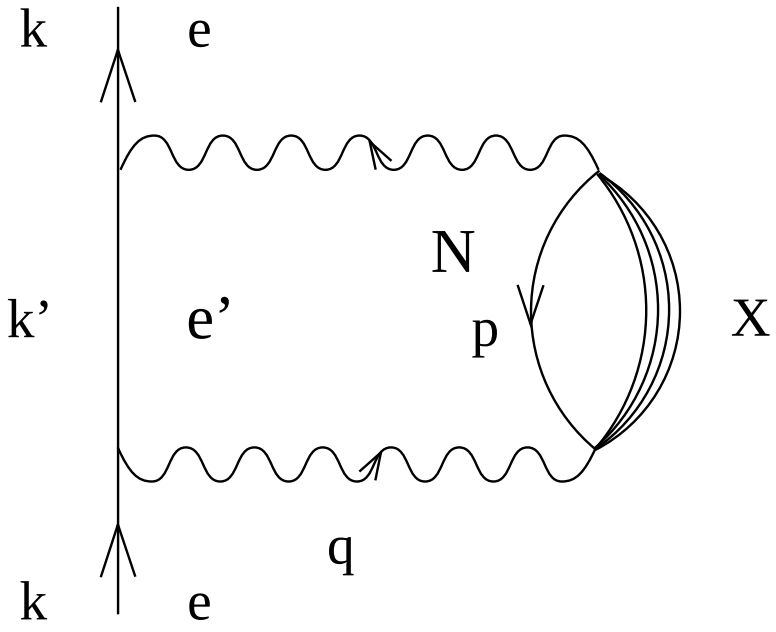

b)

Fig. 1

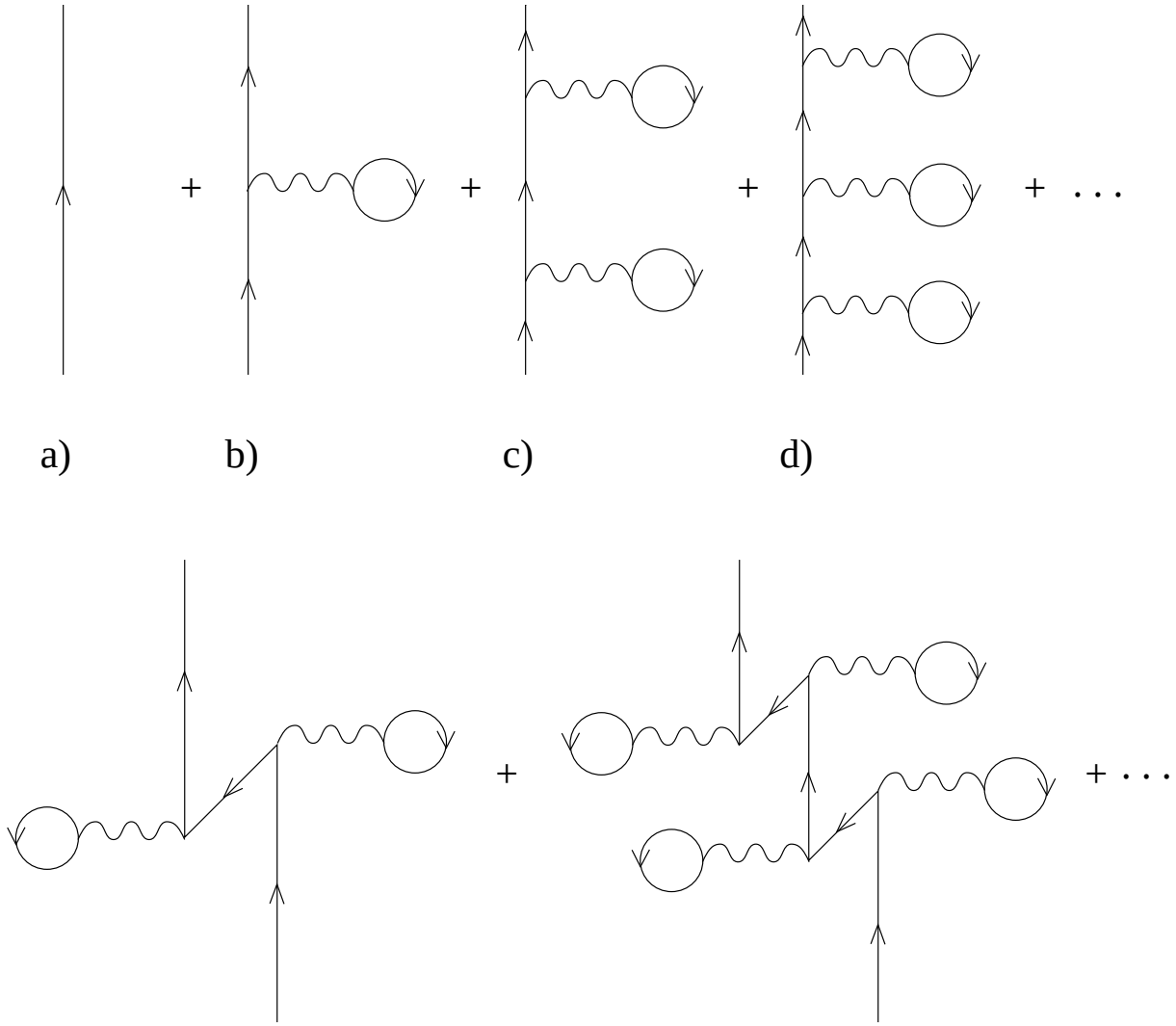

Fig. 2

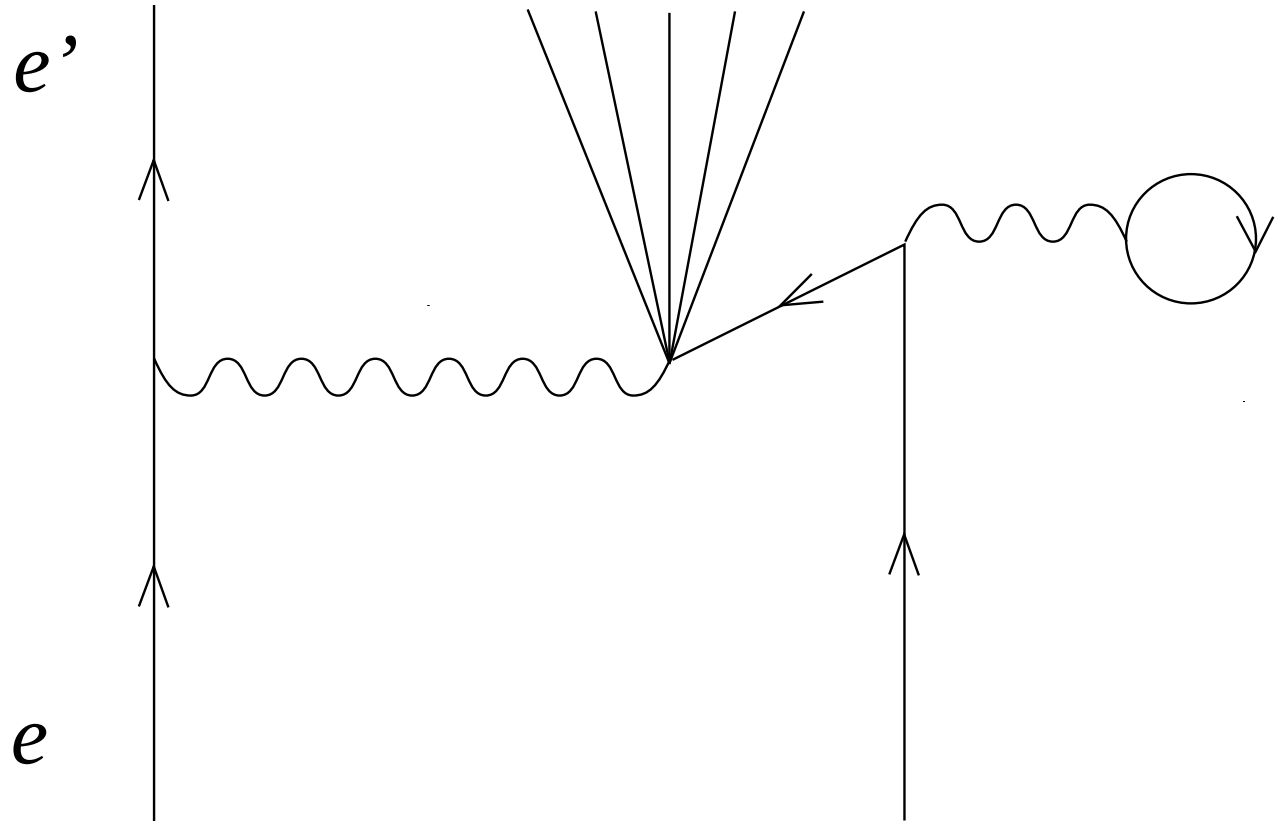

Fig. 3

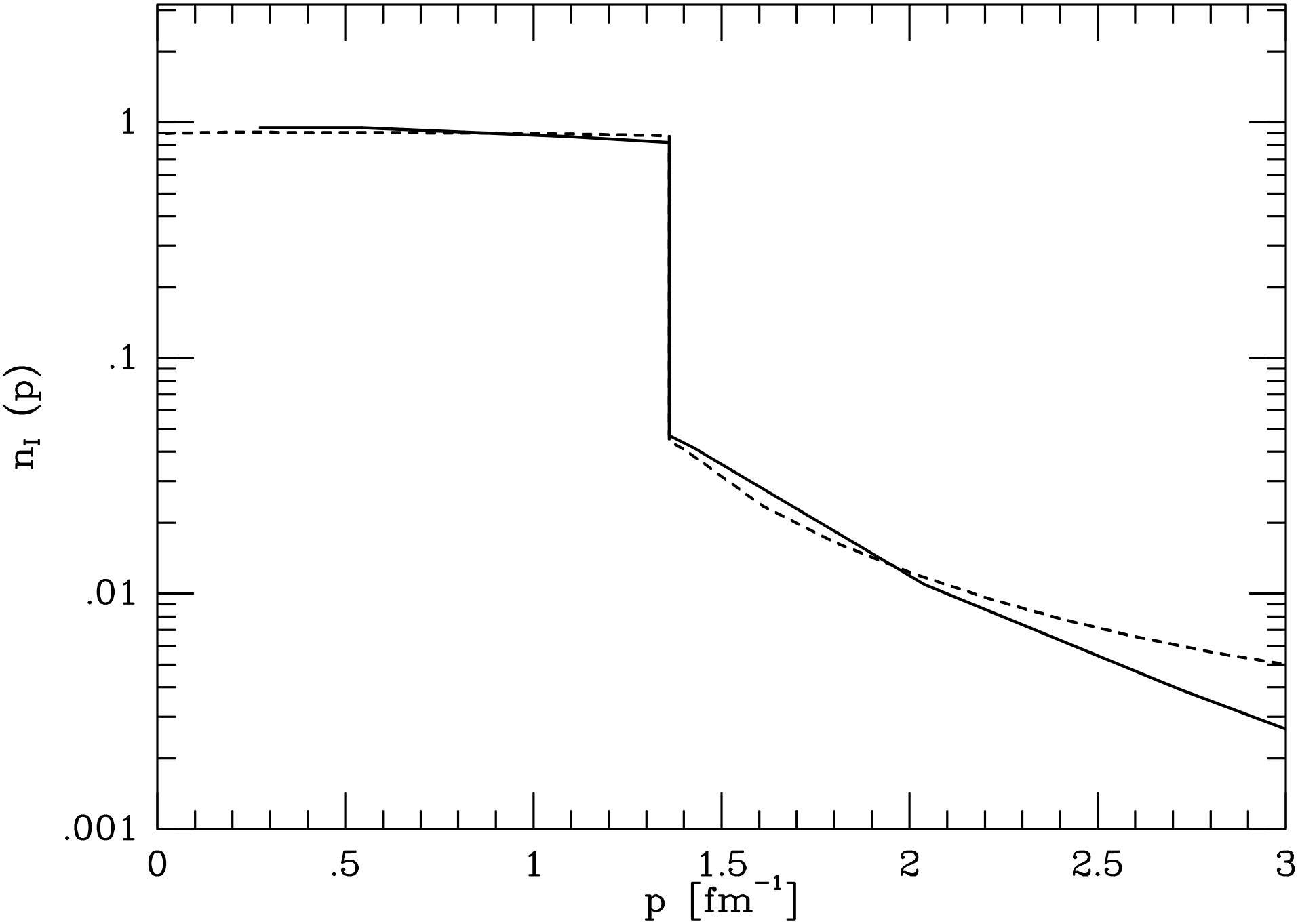
1
.1
.01
.001
n_I (p)
0
.5
1
1.5
2
2.5
3
p [fm^{-1}]

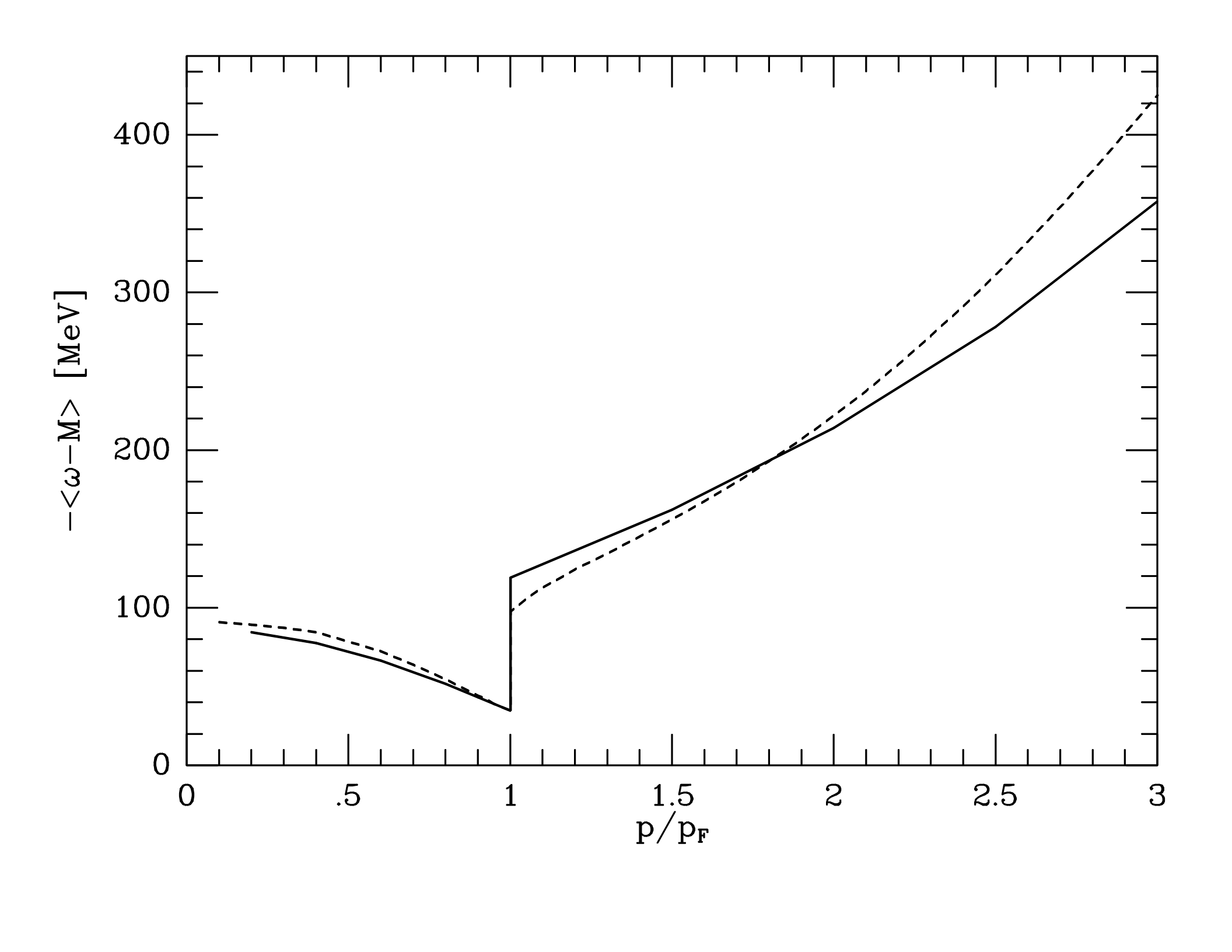
400
300
200
100
0
−<ω−M> [MeV]
0
.5
1
1.5
2
2.5
3
p/p_F

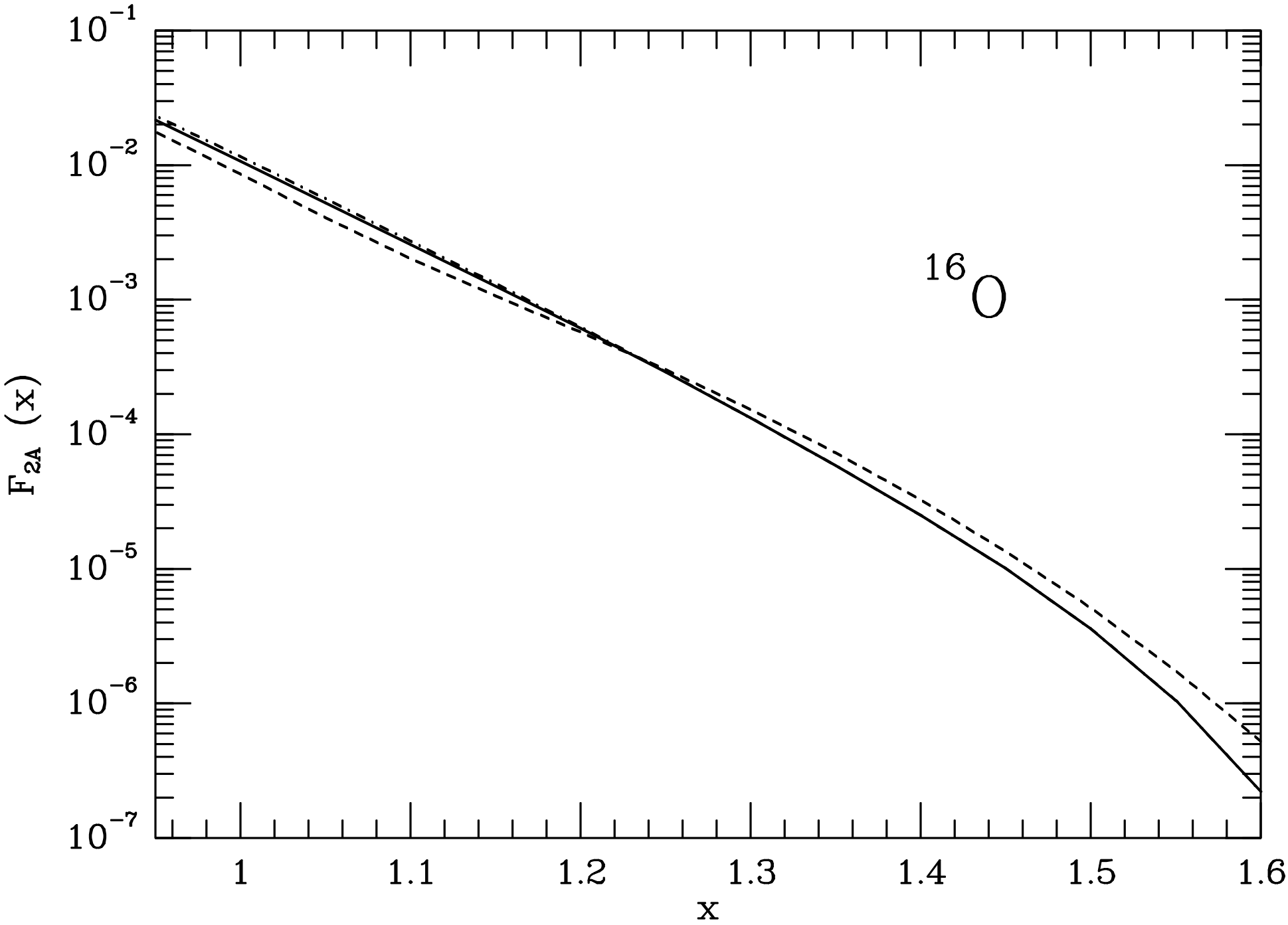
10^{-1}
10^{-2}
10^{-3}
10^{-4}
10^{-5}
10^{-6}
10^{-7}
F_{2A} (x)
^{16}O
1
1.1
1.2
1.3
1.4
1.5
1.6
x

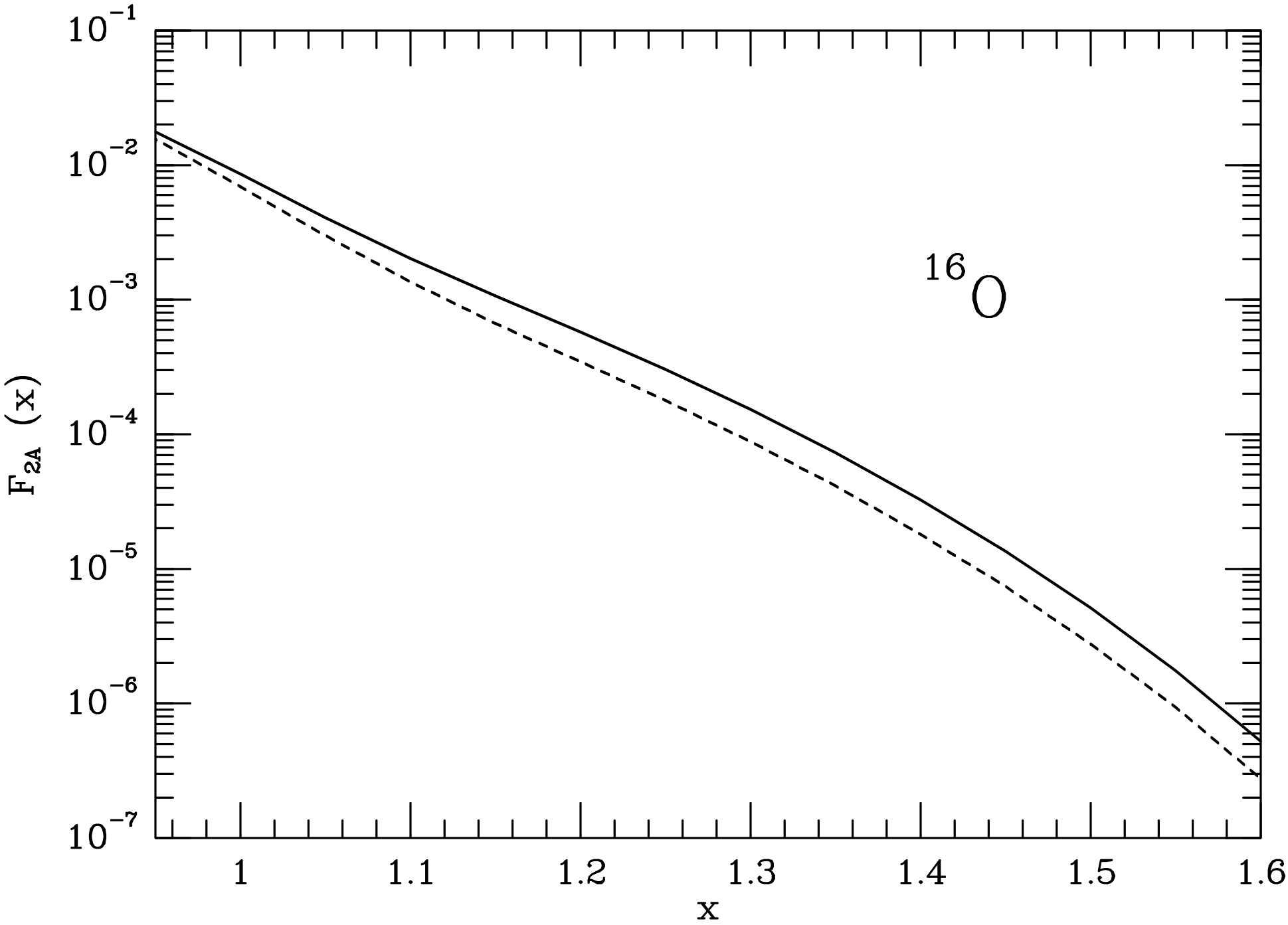
10^{-1}
10^{-2}
10^{-3}
10^{-4}
10^{-5}
10^{-6}
10^{-7}
F_{2A} (x)
^{16}O
1
1.1
1.2
1.3
1.4
1.5
1.6
x

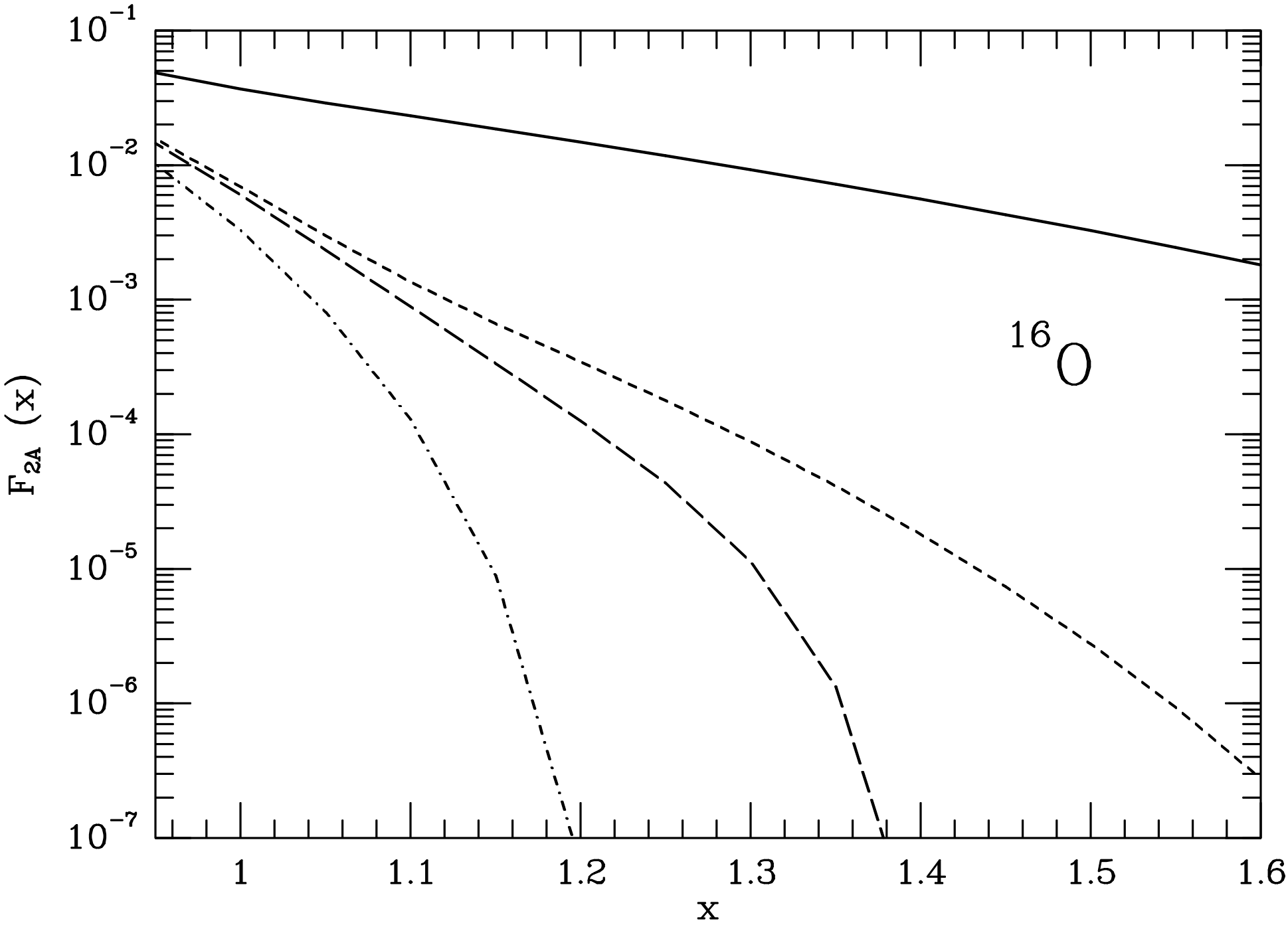
10^{-1}
10^{-2}
10^{-3}
10^{-4}
10^{-5}
10^{-6}
10^{-7}
F_{2A} (x)
^{16}O
1
1.1
1.2
1.3
1.4
1.5
1.6
x

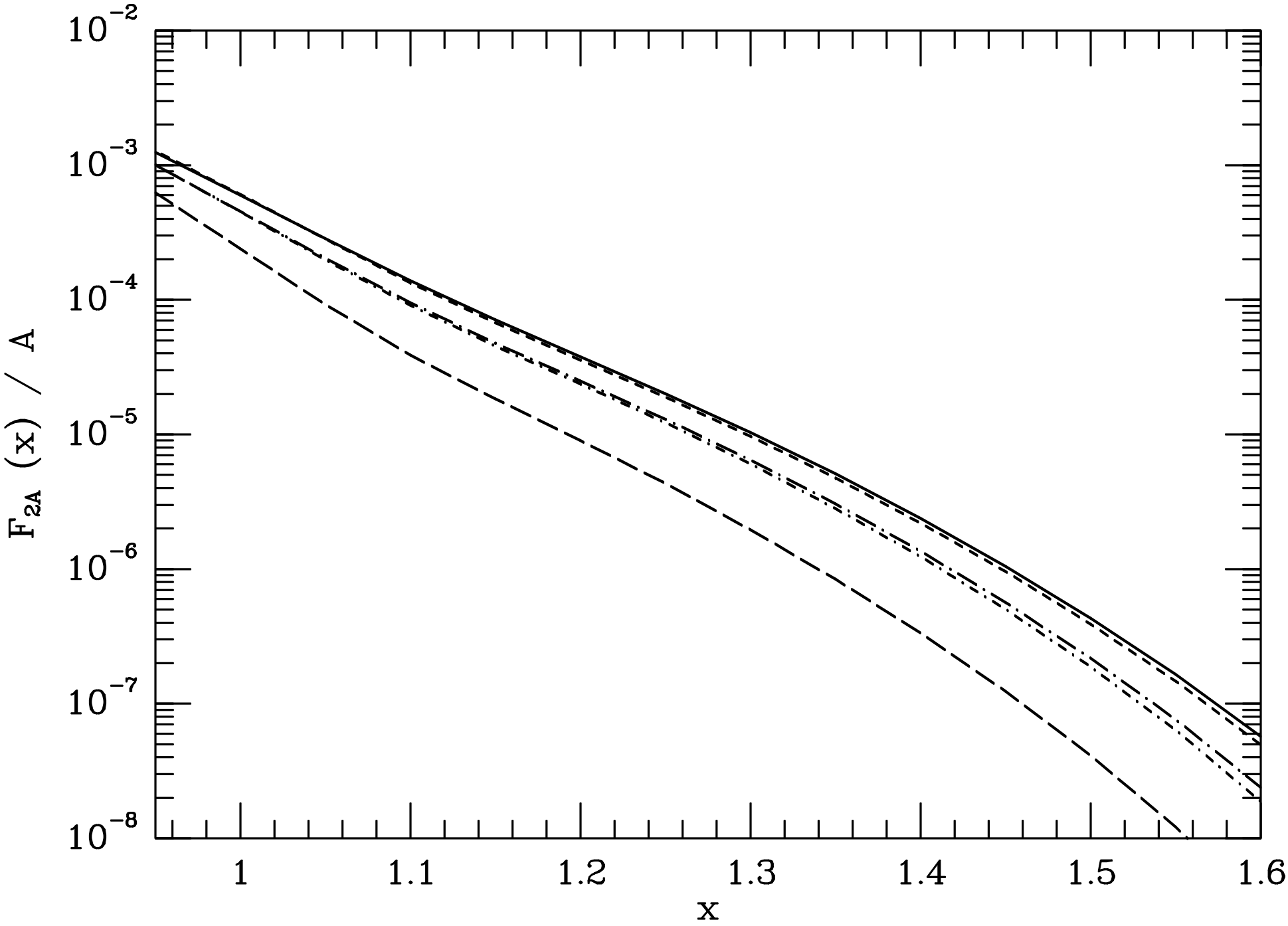
10^{-2}
10^{-3}
10^{-4}
10^{-5}
10^{-6}
10^{-7}
10^{-8}
F_{2A} (x) / A
1
1.1
1.2
1.3
1.4
1.5
1.6
x